Characterization of electromagnetically-induced-transparency-based continuous-variable quantum memories

G. Hétet, A. Peng, M. T. Johnsson, J. J. Hope, and P. K. Lam*
Australian Centre for Quantum-Atom Optics, Department of Physics, Australian National University, ACT 0200, Australia
(Received 8 January 2007; published 18 January 2008)

We present a quantum multimodal treatment describing electromagnetically induced transparency (EIT) as a mechanism for storing continuous-variable quantum information in light fields. Taking into account the atomic noise and decoherences of realistic experiments, we numerically model the propagation, storage, and readout of signals contained in the sideband amplitude and phase quadratures of a light pulse using phase space methods. An analytical treatment of the effects predicted by this model is then presented. Finally, we use quantum information benchmarks to examine the properties of the EIT-based memory and show the parameters needed to operate beyond the quantum limit.

DOI: 10.1103/PhysRevA.77.012323 PACS number(s): 03.67.Lx, 42.50.Gy

One of the steps toward the realization of quantum computation is a device that allows the coherent storage of information. The Heisenberg uncertainty principle (HUP) sets a limit on the quality of stored information that depends on direct measurement and subsequent reconstruction. Much experimental and theoretical research is directed toward quantum memories for light to circumvent this classical benchmark. To realize such memories, methods that provide a coherent interface between large atomic ensembles and light fields have been proposed.

A scheme using the off-resonant interaction of a light field with a large ensemble of three level atoms was presented in Ref. [1]. Off-resonant Faraday rotation was also used as a mechanism for mapping quantum states of light onto atoms [2]. The storage of a light field was shown to be possible by controlling the spatial distribution of atomic shifts in optically thick ensembles of three level [3,4] and two level atoms [5]. Probably the most actively studied technique to achieve a quantum memory for light utilizes electromagnetically induced transparency (EIT) [6,7].

Experiments using EIT in atoms carried out in a sodium magneto-optical trap (MOT) [6] and in hot rubidium vapor cells [8] have demonstrated the storage of a light pulse for a few milliseconds. In solid state systems a storage of more than 1 s has been achieved using photon echo techniques [9]. The quantum nature of single photon Fock states was shown to be preserved when stored and released from a MOT [10–12], and theoretical studies have proposed methods to enhance the storage efficiency in these experiments [13–15]. The delay of the two quadratures of a continuous wave beam [16,17], and the delay [18] and storage of vacuum squeezing using EIT has also recently been achieved [19,20].

Improvements in the efficacy of those system can be made with a better understanding of the sources of excess noise and loss. The transfer of the sideband statistics from optical fields to atoms also requires further investigation. In this work we develop a model describing the storage of the signals contained in the sideband amplitude and phase quadratures of a light pulse in the presence of decoherences and associated atomic noise, and use quantum information benchmarks to show the quantum nature of the transfer.

In the first part we present theoretical models that describe the multimode propagation of an amplitude and phase modulated pulse and the storage of its information onto atomic states in EIT-based memories. A numerical phase space treatment of light storage treats several sources of inefficiency present in current experiments. Maxwell-Bloch equations are then solved analytically in the weak probe approximation to explain the behavior of the atomic noise and to give an expression for the time-bandwidth product of this system in the presence of decoherence and finite atomic density.

Next, we develop criteria that quantify parameters for which EIT-based memories are able to store information in the quantum regime. Several criteria have been developed in the past to distinguish classical and quantum distributions of states in other quantum information protocols, such as teleportation or quantum cryptography. Signal-transfer coefficients T and conditional variances V_{CV} have been used as a state-independent measure to analyze the effectiveness of teleportation experiments in the presence of nonunity gain [21–23]. We propose implementing the TV diagram to define benchmarks for the storage of continuous-variable information and identify the parameters required to enable a transfer of information that outperforms any classical strategy.

I. MODEL

Previous theoretical work has characterized the efficiency of EIT as a delay line for continuous-variable quantum states [14,24]. Considering a three level atom such as the one depicted in Fig. 1, under conditions where there is a pure dephasing rate between the ground states, the information flow can be slowed down within a narrow frequency window, and no additional noise is introduced beyond that which is necessary to preserve the canonical commutation relation of the field [24]. The width of this transparency window depends on the coupling beam power, the atomic density and the ground-state decoherence rate.

Controlling the coupling beam in time allows storage of the information within the atomic sample. This storage process for continuous variables can be understood as follows. The coupling beam prepares the atoms initially in the Zee-

*ping.lam@anu.edu.au

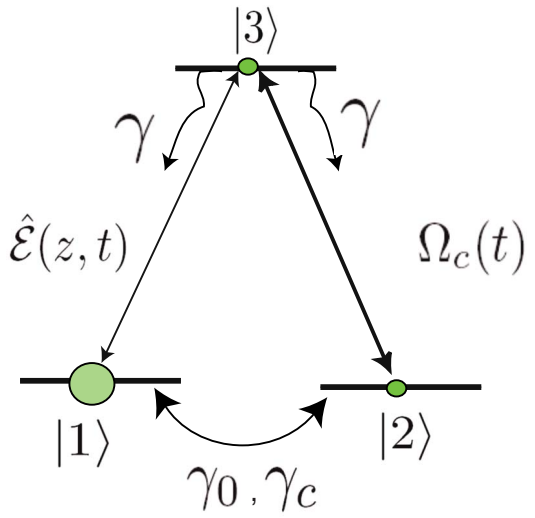

FIG. 1. (Color online) EIT level structure. $\hat{\mathcal{E}}(z,t)$ is the envelope operator of the probe field and $\Omega_c(t)$ is the coupling beam Rabi frequency. Almost all the atoms are pumped into state $|1\rangle$ initially. γ is the spontaneous emission rate from the upper state and γ_0, γ_c are mean decoherence rates between the two ground states for pure dephasing and population exchange, respectively. These two quantities are usually referred to as $1/T_2$ and $1/T_1$ in the field of magnetic resonance.

man state $|1\rangle$ through optical pumping. When a weak probe resonant with the transition $|1\rangle$–$|3\rangle$ propagates in the medium, coherences are created between the two ground states of the atoms. These coherences arise from a quantum interference between the two excitation pathways and acquire the sideband information of the probe pulse during its compression inside the medium. After the compression, most of the probe field energy has been transferred to the coupling beam and left the cell at the speed of light. At this point in time the atoms possess the frequency information of the probe within the transparency window, distributed in momentum space. When the coupling beam is turned off, the remaining energy in the probe field leaves the medium without affecting the information stored. The information will be saved provided the readout is performed before the decoherence processes have affected the atomic state. When the coupling beam is switched back on, the probe beam is regenerated with the supply of photons from the coupling beam and leaves the medium while reading the spin state of the atoms. The main constraints are that the signal has to be encoded at frequencies within the transparency window and that the compressed pulse has to fit the size of the atomic sample. When these criteria are satisfied, the efficiency of this process is close to unity. The switching of the coupling beam can be done adiabatically or abruptly if the pulse is totally compressed within the medium [6,25,26] but recent theoretical work shows that the way the coupling beam is shaped in time enhances the efficiency when the optical depth is limited [13,15].

Experimental investigation of this effect requires optical sources at or below the shot noise limit, which is only possible at some modulation frequency around a carrier. Modeling this spatiotemporal dynamics accurately therefore requires a model which contains the quantum state of a large number of modes of the light, which we provide in this paper. We solve this problem numerically and then analytically to calculate the degradation of the signal and added noise during the storage process in the presence of decoherence mechanisms. Specifically, we consider dephasing affecting the ground-state coherence and also allowing an exchange of population between the two ground states.

We approximate the atomic structure by the three level atomic Λ system shown in Fig. 1, where the two atomic ground states are degenerate and the transitions are addressed experimentally with orthogonal circular polarizations. We will consider the simultaneous storage of both quadratures of the probe when amplitude and phase modulations are encoded within the EIT bandwidth in the case where the coupling beam is switched abruptly. The preparation of this state can be achieved experimentally by passing a light pulse through amplitude and phase modulators sequentially. Provided the modulation frequency is larger than the Fourier width $\Delta\omega$ of the pulse, classical information is encoded onto its sideband ω at the shot noise limit.

The envelope of the probe field, $\hat{\mathcal{E}}(z,t)$, obeys the commutation relations $[\hat{\mathcal{E}}(z,t),\hat{\mathcal{E}}^\dagger(z',t')]=\frac{L}{c}\delta(t-z/c-(t'-z'/c))$, where L is the quantization length, taken to be the length of the cell, and c the speed of light. We are interested in the evolution of the amplitude and phase quadrature operators which will be denoted $\hat{X}^+_{\text{in}}(\omega)=\hat{\mathcal{E}}_{\text{in}}(\omega)+\hat{\mathcal{E}}^\dagger_{\text{in}}(-\omega)$ and $\hat{X}^-_{\text{in}}(\omega)=-i[\hat{\mathcal{E}}_{\text{in}}(\omega)-\hat{\mathcal{E}}^\dagger_{\text{in}}(-\omega)]$, respectively. To distinguish between the classical signal and the quantum noise, we decompose $\hat{X}^\pm_{\text{in}}(\omega)$ into

$$\hat{X}^\pm_{\text{in}}(\omega)=2\alpha^\pm_{\text{in}}(\omega)+\delta\hat{X}^\pm_{\text{in}}(\omega), \tag{1}$$

where $\alpha^\pm_{\text{in}}(\omega)$ is the coherent amplitude encoded onto the probe via optical modulation and $\delta\hat{X}^\pm_{\text{in}}(\omega)$ its quantum fluctuations.

The power spectral density $S^\pm(\omega)$ of the fluctuating signal $\hat{X}^\pm$ is the Fourier transform of its autocorrelation function, which equals [24,27]

$$S^\pm(\omega)\delta(\omega+\omega')=\frac{c}{L}\langle\hat{X}^\pm(\omega)\hat{X}^\pm(\omega')\rangle. \tag{2}$$

When normalized to the detection bandwidth, chosen to be much smaller than the applied modulation frequency, the measured power spectrum will be

$$S^\pm(\omega)=\frac{c}{L}\langle|\hat{X}^\pm(\omega)|^2\rangle \tag{3}$$

and the noise on the signal

$$V^\pm(\omega)=\frac{c}{L}\langle|\delta\hat{X}^\pm(\omega)|^2\rangle. \tag{4}$$

For the input probe state we then have $S^\pm_{\text{in}}(\omega)=4\frac{c}{L}[\alpha^\pm_{\text{in}}(\omega)]^2+V^\pm_{\text{in}}(\omega)$. The signal will be defined as $4\frac{c}{L}[\alpha^\pm_{\text{in}}(\omega)]^2$ and the noise as $V^\pm_{\text{in}}(\omega)$, which is by definition unity for a shot-noise-limited laser beam.

If this state is inefficiently stored with some frequency and quadrature-dependent loss $\eta^{\pm}(\omega)$ and if some excess noise with amplitude $V^{\pm}_{\text{noise}}(\omega)$ is generated by the memory, we will have

$$S^{\pm}_{\text{out}} = \eta^{\pm}(\omega) S^{\pm}_{\text{in}} + 1 - \eta^{\pm}(\omega) + V^{\pm}_{\text{noise}}(\omega). \tag{5}$$

The term $1-\eta^{\pm}(\omega)$ corresponds to uncorrelated vacuum noise, common to any system in the presence of loss. This vacuum noise is necessary to preserve the commutation relations of the output state. The excess noise $V^{\pm}_{\text{noise}}(\omega)$ transforms an initial coherent state, where $V^{\pm}_{\text{in}}(\omega)=1$ into a mixed state where $V^{\pm}_{\text{out}}(\omega)=1+V^{\pm}_{\text{noise}}(\omega)>1$.

In the following sections we will calculate $\eta^{\pm}(\omega)$ and $V^{\pm}_{\text{noise}}(\omega)$ using phase space simulations in the positive-P representation, and use a simplified model that identifies the origin of the excess noise and describe the light storage and retrieval efficacy. We treat the probe beam as a general quantized field with longitudinal spatial dependence z, and the coupling beam Ω_c as a classical field. The atoms are all prepared in state $|1\rangle$ before the probe enters the cell via optical pumping induced by Ω_c.

In this study we assume the coupling beam Rabi frequency to be 10^4 times larger than that of the probe, ensuring that no atoms will move into state $|2\rangle$ due to optical pumping induced by the probe, and the coupling beam will not be depleted throughout the storage process. Its dependence on z will therefore be ignored in this treatment. The validity of this approximation in the presence of decoherence is discussed in Sec. I B 1. When both beams are of comparable strength and both are treated as quantum fields, a strong correlation develops between them [28–32]. As we are well away from this regime in our system, this correlation will not affect the quantum statistics of our probe, allowing us to treat the coupling beam as a classical field.

The master equation of this system is

$$\frac{\partial}{\partial t}\hat{\rho} = \frac{1}{i\hbar}[\hat{\mathcal{H}}_{\text{int}}, \hat{\rho}] + \mathcal{L}_{31}[\hat{\rho}] + \mathcal{L}_{32}[\hat{\rho}] + \mathcal{L}^{\text{deph}}_{[1,2]}[\hat{\rho}] + \mathcal{L}^{\text{coll}}_{[1,2]}[\hat{\rho}], \tag{6}$$

where $\hat{\rho}$ is the reduced density matrix of the optical field and atomic variables and $\hat{\mathcal{H}}_{\text{int}}$ is the interaction Hamiltonian. We define locally averaged atomic dipole operators $\hat{\sigma}_{ij}(z,t)$ for the $|i\rangle - |j\rangle$ transition given by [7,24]

$$\hat{\sigma}_{ij}(z,t) = \frac{1}{n\mathcal{A}\delta z}\sum_{z_k \in \delta z} \hat{\sigma}^k_{ij}(z,t), \tag{7}$$

where $\mathcal{A}$ is the cross-sectional area of the beam, n the atomic density, and δz an infinitesimal slice of the medium containing N atoms. In the rotating wave approximation, the interaction Hamiltonian is then

$$\hat{\mathcal{H}}_{\text{int}} = -\int \frac{N\hbar}{L}[g\hat{\mathcal{E}}(z,t)\hat{\sigma}_{31}(z,t) + \Omega_c(t)\hat{\sigma}_{32}(z,t) + \text{H.c.}]dz, \tag{8}$$

where g is the coupling strength on the probe transition. The $\mathcal{L}_{i3}$ are Liouvillians modeling the decays due to spontaneous emission from the upper state $|3\rangle$, and are defined by

$$\mathcal{L}_{i3}[\hat{\rho}] = \gamma \sum_{z_k \in \delta z}\left(\hat{\sigma}^k_{i3}\hat{\rho}\hat{\sigma}^k_{3i} - \frac{1}{2}\hat{\sigma}^k_{i3}\hat{\sigma}^k_{3i}\hat{\rho} - \frac{1}{2}\hat{\rho}\hat{\sigma}^k_{i3}\hat{\sigma}^k_{3i}\right), \tag{9}$$

where for simplicity we assume the decay rates γ from the upper state to be the same for both transitions.

$\mathcal{L}^{\text{deph}}_{[1,2]}$ accounts for an off-diagonal dephasing rate γ_0 affecting the ground-state coherence and arises from elastic collisions or atoms moving in and out of the interaction region defined by the probe beam quantized mode. Its expression is

$$\mathcal{L}^{\text{deph}}_{[1,2]}[\hat{\rho}] = \gamma_0 \sum_{z_k \in \delta z}\left(\hat{\sigma}^k_{11}\hat{\rho}\hat{\sigma}^k_{11} - \frac{1}{2}\hat{\sigma}^k_{11}\hat{\sigma}^k_{11}\hat{\rho} - \frac{1}{2}\hat{\rho}\hat{\sigma}^k_{11}\hat{\sigma}^k_{11}\right) + \gamma_0 \sum_{z_k \in \delta z}\left(\hat{\sigma}^k_{22}\hat{\rho}\hat{\sigma}^k_{22} - \frac{1}{2}\hat{\sigma}^k_{22}\hat{\sigma}^k_{22}\hat{\rho} - \frac{1}{2}\hat{\rho}\hat{\sigma}^k_{22}\hat{\sigma}^k_{22}\right). \tag{10}$$

This term does not affect the atomic population. If the pumping preparation is not optimum or if inelastic collisions are non-negligible, a population exchange term $\mathcal{L}^{\text{coll}}_{[1,2]}$ needs to be introduced.

It is defined as

$$\mathcal{L}^{\text{coll}}_{[1,2]}[\hat{\rho}] = \gamma_c \sum_{z_k \in \delta z}\left(\hat{\sigma}^k_{12}\hat{\rho}\hat{\sigma}^k_{21} - \frac{1}{2}\hat{\sigma}^k_{12}\hat{\sigma}^k_{21}\hat{\rho} - \frac{1}{2}\hat{\rho}\hat{\sigma}^k_{12}\hat{\sigma}^k_{21}\right) + \gamma_c \sum_{z_k \in \delta z}\left(\hat{\sigma}^k_{21}\hat{\rho}\hat{\sigma}^k_{12} - \frac{1}{2}\hat{\sigma}^k_{21}\hat{\sigma}^k_{12}\hat{\rho} - \frac{1}{2}\hat{\rho}\hat{\sigma}^k_{21}\hat{\sigma}^k_{12}\right). \tag{11}$$

$\mathcal{L}^{\text{coll}}_{[1,2]}[\hat{\rho}]$ also affects the off-diagonal terms in the density matrix in the same way as $\mathcal{L}^{\text{deph}}_{[1,2]}[\hat{\rho}]$, but as the sources of these two decoherence processes are different we monitor them separately. It should be noted that this last term does not account for a pure loss of atoms out of the system, due to possible atomic motion out of the interaction region or atoms moving into other hyperfine states. We also assume the mean dephasing rates describing quantum jumps from $|1\rangle$ to $|2\rangle$ to be the same as the mean rates describing quantum jumps from $|2\rangle$ to $|1\rangle$ for simplicity. The ratio between γ_0 and γ_c depends on the atomic system used. In a cool enough atomic sample where the mean free path of the atoms is on the order of the probe beam size γ_0 would, for example, be dominant. Those two quantities have recently been characterized experimentally in a vapor cell containing a buffer gas [33]. It indeed appeared that γ_0 was the main source of dephasing with γ_c playing a minor role.

A. Stochastic simulations

To model this system, we used stochastic phase space methods, and worked with the positive-P representation [34]. This phase space representation is computationally intensive but has the advantage of being exact as opposed to the truncated Wigner representation. We choose the following normal ordering of the operators:

$$(\hat{\mathcal{E}}^{\dagger}, \hat{\sigma}_{13}^{\dagger}, \hat{\sigma}_{23}^{\dagger}, \hat{\sigma}_{12}^{\dagger}, \hat{\sigma}_{33}, \hat{\sigma}_{22}, \hat{\sigma}_{11}, \hat{\sigma}_{13}, \hat{\sigma}_{23}, \hat{\sigma}_{12}, \hat{\mathcal{E}}) \tag{12}$$

and define

$$\hat{\Xi}(\underline{\lambda}, z) = \prod_i e^{\lambda_i \hat{O}_i(z)}, \tag{13}$$

where $\hat{O}_i(z)$ refers to the ith operator in our normally ordered definition and $\underline{\lambda} = (\lambda_0 \cdots \lambda_i \cdots \lambda_{11})$ is a real vector. The normally ordered characteristic function [35] is then

$$\chi(\underline{\lambda}, z) = \mathrm{Tr}[\hat{\rho}\hat{\Xi}(\underline{\lambda}, z)]. \tag{14}$$

The equations of motion for $\chi(\underline{\lambda}, z)$ are calculated using the master Eq. (6) and the commutation properties of the atomic and field operators. By taking the Fourier transform of the characteristic function equations of motion, and assuming a large number of atoms in each slice δz, a Fokker-Planck equation can be found. We then derive a set of nine complex-valued Ito stochastic differential equations (SDE) describing the atomic dynamics, with 18 uncorrelated noise terms arising from atomic fluctuations. Their expressions are given in Appendix A. The Stratonovitch corrections used in the numerical simulations are also listed in the appendix, but they are small compared to all the other variables and are not included in the SDE. The Maxwell equations for the probe envelope in a moving frame at the speed of light are

$$\frac{\partial}{\partial z}\alpha(z,t) = \frac{igN}{c}\sigma_3(z,t), \tag{15}$$

$$\frac{\partial}{\partial z}\beta(z,t) = \frac{igN}{c}\sigma_{11}(z,t), \tag{16}$$

where the c numbers α and β represent the operators $\hat{\mathcal{E}}$ and $\hat{\mathcal{E}}^{\dagger}$, and σ_3, σ_{11} correspond to the atomic operators $\hat{\sigma}_{13}$, $\hat{\sigma}_{13}^{\dagger}$ (this naming convention follows the one introduced in Appendix A).

The evolution of α and β in space and time is computed when amplitude and phase modulations at a frequency 0.005γ are encoded onto a $50/\gamma$ long coherent input state; the envelope of the field then shows two cycles in both quadratures. We numerically evaluate the expectation values of the two quadrature operators $\langle \hat{X}^{+}(z,t)\rangle = \overline{\alpha(z,t)+\beta(z,t)}$ and $\langle \hat{X}^{-}(z,t)\rangle = -i\overline{[\alpha(z,t)-\beta(z,t)]}$ and their noise spectrum $S^{\pm}(\omega) = \frac{c}{L}\overline{X^{\pm}(z,\omega)X^{\pm}(z,-\omega)}$, where the averaging is done over a large number of trajectories in phase space. The noise floor $V^{\pm}(z,\omega)$ is obtained by turning off the signal on the probe. We solved these stochastic equations using the numerical package XMDS [36] and chose parameters realistic to atom optics experiments with ^{87}Rb atoms. The atomic density was chosen to be 10^{12} cm^3 with a sample total length of 12 cm. At the moment the pulse is inside the medium, the coupling beam is switched off abruptly and turned back on $50/\gamma$ later. For these particular simulations, we chose a dephasing rate $\gamma_0 = 250$ Hz and an inelastic scattering rate $\gamma_c = 100$ Hz.

Figure 2 shows the results of this simulation where two quadratures of the multimode field have been stored in the

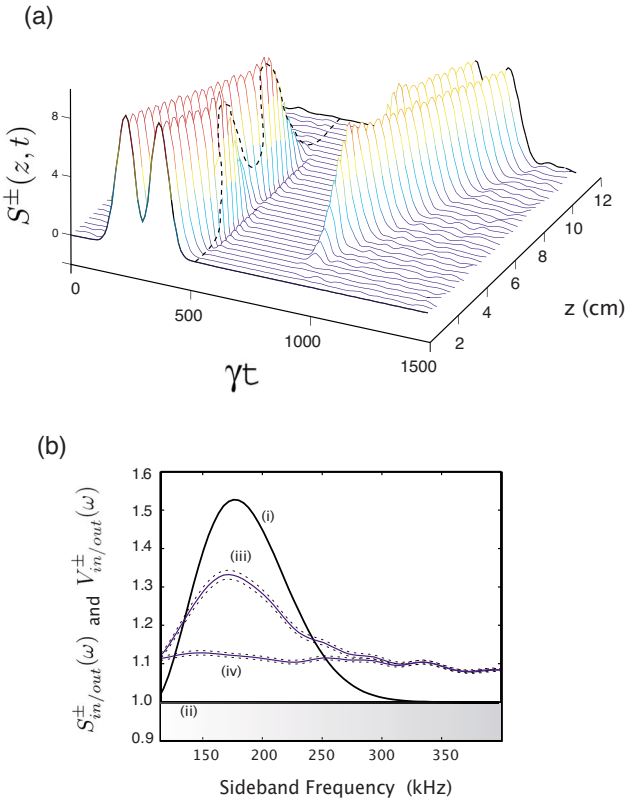

FIG. 2. (Color online) Phase space numerical simulations of quantum information storage using EIT. Amplitude and phase modulations at 190 kHz are applied to the pulse. The decoherence rates are $\gamma_0 = 250$ Hz, $\gamma_c = 100$ Hz. (a) 3D graph showing the storage of the probe amplitude quadrature on a time-space grid. (b) Variances of the input and output fields for the amplitude and phase quadratures, with 1 corresponding to the quantum noise limit. (i)–(iii) is the power spectrum of the input and output states and (ii)–(iv) are the noise floor of the input and output states. The dashed lines corresponds to statistical standard deviations. These simulations are the average of 2000 trajectories.

presence of atomic noise. The stochastic simulations were averaged over 2000 trajectories. Figure 2(a) shows the propagation of the amplitude quadrature of the modulated pulse through the cell. The results are identical for the phase quadrature and are not shown here. We can see that the EIT memory preserves the shape of the signal with minimal distortion. To better quantify this we plot the power spectrum of the input and output fields in Fig. 2(b). The asymmetry in the transmission reveals a frequency-dependent absorption of the pulse as it propagates through the system, characteristic of the EIT Lorentzian transmission window. For these simulations, 60% of the classical signal is absorbed but also extra noise is added to the field. Using the previously defined notation the transmission $\eta^{\pm}(\omega) = 0.40$ and the excess noise $V^{\pm}_{\mathrm{noise}}(\omega) = 0.12$. We will see in Sec. II if these conditions correspond to a quantum memory regime and describe the origin of the noise in the following section.

It should be noted here that an iterative procedure was recently proposed to optimize the coupling beam shape and power in Ref. [13]. We also performed some simulations by

shaping the control field and noticeable improvements were found on the transmission and noise of the signal. The in depth study of these effects were done during the course of this work in Ref. [13] and are beyond the scope of our study. In this paper, we chose our (time independent) coupling beam Rabi frequency by maximizing the output signal without decoherence, i.e., we found a trade off between off line center absorption and the compression of the pulse required to fit the sample. In this case the efficiency η was found to be 80%, only limited by the lack of optical depth. At higher densities and optimized coupling beam strength, we found a transmission close to unity. Such time-bandwidth considerations are developed formally in Sec. I B 2.

B. Interpretation

In this section we provide an explanation of the results found in the above phase space simulations. We first discuss the effects of decoherences on the losses and atomic noise introduced during the light propagation. We will show that excess noise can be understood as a preservation of the canonical commutation relations of the field in the presence of gain in the medium. We will quantify this by solving the Heisenberg-Langevin equations in the weak probe approximation in the case of information delay, and compare it with a more general theory of amplification and attenuation. We then describe the mapping and readout of the information encoded on the probe, derive boundaries for optimum storage, and quantify the maximum information that can be stored in this system. As in our numerical simulations, the process will be solved with the coupling beam switched off abruptly.

1. The role of decoherences

We will here focus on the noise properties of the EIT as a delay line to explain the excess noise observed. From the interaction Hamiltonian Eq. (8), we can obtain a set of Heisenberg-Langevin equations

$$\dot{\hat{\sigma}}_{11} = \gamma\hat{\sigma}_{33} + \gamma_c(\hat{\sigma}_{22} - \hat{\sigma}_{11}) - ig\hat{\mathcal{E}}\hat{\sigma}_{31} + ig^*\hat{\mathcal{E}}^\dagger\hat{\sigma}_{13} + \hat{F}_{11},$$

$$\dot{\hat{\sigma}}_{22} = \gamma\hat{\sigma}_{33} + \gamma_c(\hat{\sigma}_{11} - \hat{\sigma}_{22}) - i\Omega_c\hat{\sigma}_{32} + i\Omega_c^*\hat{\sigma}_{23} + \hat{F}_{22},$$

$$\dot{\hat{\sigma}}_{13} = -(\gamma + \gamma_0/2 + \gamma_c/2)\hat{\sigma}_{13} + ig\hat{\mathcal{E}}(\hat{\sigma}_{11} - \hat{\sigma}_{33}) + i\Omega_c\hat{\sigma}_{12} + \hat{F}_{13},$$

$$\dot{\hat{\sigma}}_{32} = -(\gamma + \gamma_0/2 + \gamma_c/2)\hat{\sigma}_{32} + i\Omega_c^*(\hat{\sigma}_{33} - \hat{\sigma}_{22}) - i\ g^*\hat{\mathcal{E}}^\dagger\hat{\sigma}_{12} + \hat{F}_{32},$$

$$\dot{\hat{\sigma}}_{12} = -(\gamma_0 + \gamma_c)\hat{\sigma}_{12} - ig\hat{\mathcal{E}}\hat{\sigma}_{32} + i\Omega_c^*\hat{\sigma}_{13} + \hat{F}_{12},$$

$$\frac{\partial}{\partial z}\hat{\mathcal{E}} = \frac{igN}{c}\hat{\sigma}_{13} \tag{17}$$

and $\dot{\hat{\sigma}}_{33} = -(\dot{\hat{\sigma}}_{11} + \dot{\hat{\sigma}}_{22})$. We have included the decays of the atomic dipole operators, and their associated Langevin noise operators $\hat{F}_{ij}$ describing the coupling of the atoms to vacuum modes of large reservoirs. The expressions for the Langevin correlations are calculated using the Einstein generalized equations [24,37]. and the nonzero contributions are given in Appendix B. The system of Eqs. (17) will be solved to first order in $\hat{\mathcal{E}}$, γ_c/γ, and γ_0/γ. To ensure an efficient pumping into the dark state, therefore an optimum electromagnetically induced transparency, we will also assume $|\Omega_c|^2 \gg (\gamma\gamma_0, \gamma\gamma_c)$.

We first perform a steady-state analysis of this system in this approximate regime. From the last three Bloch equations, we get a relation between the coherences and the populations terms. Using this result, the first two Bloch equations and the population preservation relation, an expression for the populations can be obtained to first order in the weak probe approximation. Assuming the coupling beam Rabi frequency to be real and satisfying $\Omega_c^2 \gg (\gamma\gamma_0, \gamma\gamma_c)$, the atomic steady states are finally found to first order in γ_c/γ

$$\langle\hat{\sigma}_{11}\rangle = 1 - 2\frac{\gamma_c}{\gamma}, \quad \langle\hat{\sigma}_{22}\rangle = \frac{\gamma_c}{\gamma}, \quad \langle\hat{\sigma}_{33}\rangle = \frac{\gamma_c}{\gamma},$$

$$\langle\hat{\sigma}_{12}\rangle = -\frac{g\langle\hat{\mathcal{E}}\rangle}{\Omega_c}, \quad \langle\hat{\sigma}_{13}\rangle = \frac{ig\gamma_0}{\Omega_c^2}\langle\hat{\mathcal{E}}\rangle, \quad \langle\hat{\sigma}_{23}\rangle = \frac{i\gamma_c}{\Omega_c}. \tag{18}$$

We note that the atoms are not fully pumped in the state $|1\rangle$ due to population exchange γ_c, and therefore a nonzero dipole $\langle\hat{\sigma}_{23}\rangle$ appears on the coupling beam transition. In this paper, however, we have assumed that the coupling beam is not depleted. In order for these solutions to be consistent, we then need to find the regimes where the coupling beam is negligibly absorbed. We do so by solving the following Maxwell equation for the coupling beam propagation:

$$\frac{\partial\Omega_c(z)}{\partial z} = \frac{ig^2N}{c}\langle\hat{\sigma}_{23}\rangle, \tag{19}$$

the solution for which is

$$\Omega_c^2(z) = \Omega_c^2(0) + 2d\gamma\gamma_c z/L, \tag{20}$$

where $d = \frac{g^2NL}{\gamma c}$ is the optical depth of the medium seen by the probe field without control field and decoherence. Although the coupling beam intensity is absorbed linearly through the medium, a negligible depletion is guaranteed under the condition

$$\frac{\Omega_c^2}{\gamma\gamma_c} \gg 2d \tag{21}$$

which we will require in all the following calculations. This condition is verified in the above numerical analysis and the one presented in the last section. We also note that because of the pure dephasing γ_0 a dipole $\langle\hat{\sigma}_{13}\rangle$ is created on the probe transition. A portion of the mean probe field is then absorbed by the medium by an amount $e^{-\alpha_0 L}$, where $\alpha_0 = \frac{gN}{c}\frac{\gamma_0}{\Omega_c^2}$.

We will now calculate the evolution of the probe quantum field as it propagates through the medium in the same approximate regime. To simplify the equations, the fast-

decaying atomic variables will be adiabatically eliminated ($1/T \ll \gamma$, where T is a characteristic time scale), making these equations valid over time scales larger than the spontaneous emission decay time, which is the regime of interest for EIT. It was noticed in Ref. [13] that this adiabatic approximation is actually less severe even when ground-state decoherence is taken into account. By solving the Maxwell equation for the probe field and substituting it back into the equation of motion for $\hat{\sigma}_{13}$ we find that $1/T \ll \gamma(1+d)$ is, in fact, a sufficient condition.

We follow the same procedure as in Ref. [24] and solve the equations in the Fourier domain. Using the steady state solutions listed above, we can eliminate the second-order terms in the probe field and negligible Langevin noise contributions using Appendix B.

The Maxwell equation for the field amplitude quadratures can be solved to give

$$\hat{\mathcal{E}}(z,\omega) = \hat{\mathcal{E}}(0,\omega)e^{-\Lambda(\omega)z} - \frac{gN}{c}\int_0^z ds\ e^{-\Lambda(\omega)(z-s)}\frac{\omega - i\gamma_d}{\mu(\omega)}\hat{F}_{12}(s,\omega) + \frac{gN}{c}\int_0^z ds\ e^{-\Lambda(\omega)(z-s)}\frac{i\Omega_c}{\mu(\omega)}\hat{F}_{13}(s,\omega), \quad (22)$$

where $\mu(\omega)=\Omega_c^2 - i\omega(\gamma+\gamma_d/2)$; $\gamma_d=\gamma_0+\gamma_c$ is the total decoherence rate and the susceptibility of the medium is given by

$$\Lambda(\omega) = \frac{g^2 N}{c}\frac{(\gamma_d - i\omega)\langle\hat{\sigma}_{11}-\hat{\sigma}_{33}\rangle - i\langle\hat{\sigma}_{32}\rangle\Omega_c}{\mu(\omega)}. \quad (23)$$

The first part of Eq. (22) describes the absorption and phase shift of the probe propagating with a group velocity given by $v_g=-\omega/\mathrm{Im}[\Lambda(\omega)]$ inside the EIT medium. The last two terms in Eq. (22) correspond to atomic noise added to the field due to decoherence.

We now calculate the power spectrum of the output state as a function of the input state using Eqs. (2) and (22) and the Langevin correlations listed in Appendix B. First we note that

$$2\mathrm{Re}[\Lambda(\omega)] = \frac{\Omega_c^2\langle[\hat{F}_{12},\hat{F}_{12}^\dagger]\rangle + \omega^2\langle[\hat{F}_{13},\hat{F}_{13}^\dagger]\rangle}{|\mu(\omega)|^2}, \quad (24)$$

which links the linear absorption with the atomic noise, a direct consequence of the fluctuation dissipation theorem. This allows us to obtain

$$S^{\pm}(z,\omega) = \eta(z,\omega)S_{\mathrm{in}}^{\pm}(\omega) + [1-\eta(z,\omega)](1+N_f), \quad (25)$$

where $\eta(z,\omega)=e^{-2\mathrm{Re}[\Lambda(\omega)]z}$, and

$$N_f = 2\frac{\Omega_c^2\langle\hat{F}_{12}^\dagger\hat{F}_{12}\rangle + \omega^2\langle\hat{F}_{13}^\dagger\hat{F}_{13}\rangle}{\Omega_c^2\langle[\hat{F}_{12},\hat{F}_{12}^\dagger]\rangle + \omega^2\langle[\hat{F}_{13},\hat{F}_{13}^\dagger]\rangle} = \frac{4\gamma_c\Omega_c^2}{2\gamma_0\Omega_c^2 + \omega^2(2\gamma+\gamma_0-3\gamma_c)}. \quad (26)$$

We note that the noise power spectrum is phase independent, indicating that the response of the medium is the same for both quadratures of the field. The normally ordered Langevin correlations are responsible for excess noise on the output field. Using the notation defined previously we have $V_{\mathrm{noise}}^{\pm}(z,\omega)=[1-\eta(z,\omega)]N_f$. When they are all zero, $N_f=0$, and the preservation of the commutation relations of the output field is ensured by the antinormally ordered Langevin correlations as $V^{\pm}(z,\omega)=1$ in that case. From the Langevin correlations calculated in Appendix B, we see that $\langle\hat{F}_{13}^\dagger\hat{F}_{13}\rangle=0$ to first order in γ_c/γ. This means that the spontaneous emission does not contribute to the excess noise. However, $\langle\hat{F}_{12}^\dagger\hat{F}_{12}\rangle=4\gamma_c$ so the only noise contribution arises from the population shuffling terms.

In order to understand why population exchange between the ground states is responsible for noise, we will simplify the equations further and concentrate on sideband frequencies close to the carrier. We first solve for the steady states with the population shuffling terms $\gamma_c(\hat{\sigma}_{11}-\hat{\sigma}_{22})$ and $\gamma_c(\hat{\sigma}_{22}-\hat{\sigma}_{11})$ as the only source of decoherence. We find a new solution for the atomic polarization

$$\langle\hat{\sigma}_{13}\rangle = -\frac{i\gamma_c}{\Omega_c^2}\langle\hat{\mathcal{E}}\rangle \quad (27)$$

and insert it into the Maxwell equation to obtain

$$\langle\hat{\mathcal{E}}(z)\rangle = \langle\hat{\mathcal{E}}_{\mathrm{in}}\rangle e^{az}, \quad (28)$$

where

$$a = \frac{gN}{c}\frac{\gamma_c}{\Omega_c^2}. \quad (29)$$

This expression corresponds to a population exchange driven amplification of the probe field inside the medium, the energy for which will be provided by the coupling beam, up to a limit set by Eq. (21).

This shuffling term alone is, however, not physically realistic. As can be seen from the stochastic equation listed in Appendix B and Eqs. (17), the Liouvillian $\mathcal{L}_{[1,2]}^{\mathrm{coll}}$ also includes an off diagonal ground-state dephasing with mean rate γ_c giving an extra linear loss $\alpha_c=\frac{gN}{c}\frac{\gamma_c}{\Omega_c^2}$ similar to α_0. When solving for the steady state in this case, we find the net transmission close to zero frequency to be unity. The losses in fact exactly compensate for the gain, and the EIT medium no longer performs amplification. Even though the transmission that includes $\mathcal{L}_{[1,2]}^{\mathrm{coll}}$ gives no net amplification, this underlying gain term results in excess noise on the output.

Using Eq. (26) close to $\omega=0$ and for $\gamma_0\neq 0$ we find the noise to be

$$V_{\mathrm{noise}} = 2\frac{\gamma_c}{\gamma_0}(1-e^{(a-\alpha_0-\alpha_c)z}) \quad (30)$$

and for $\gamma_0=0$, $V_{\mathrm{noise}}=2az$. A similar expression can in fact be found in the theory of two beam coupling developed in Ref. [38]. The presence of excess noise on the output field can be recognized from the theory of phase-insensitive quantum amplifiers. In Ref. [39] the signal to noise ratio of the optical field was shown to degrade in the presence of gain, and extra noise has to be inserted in the field equations to preserve the

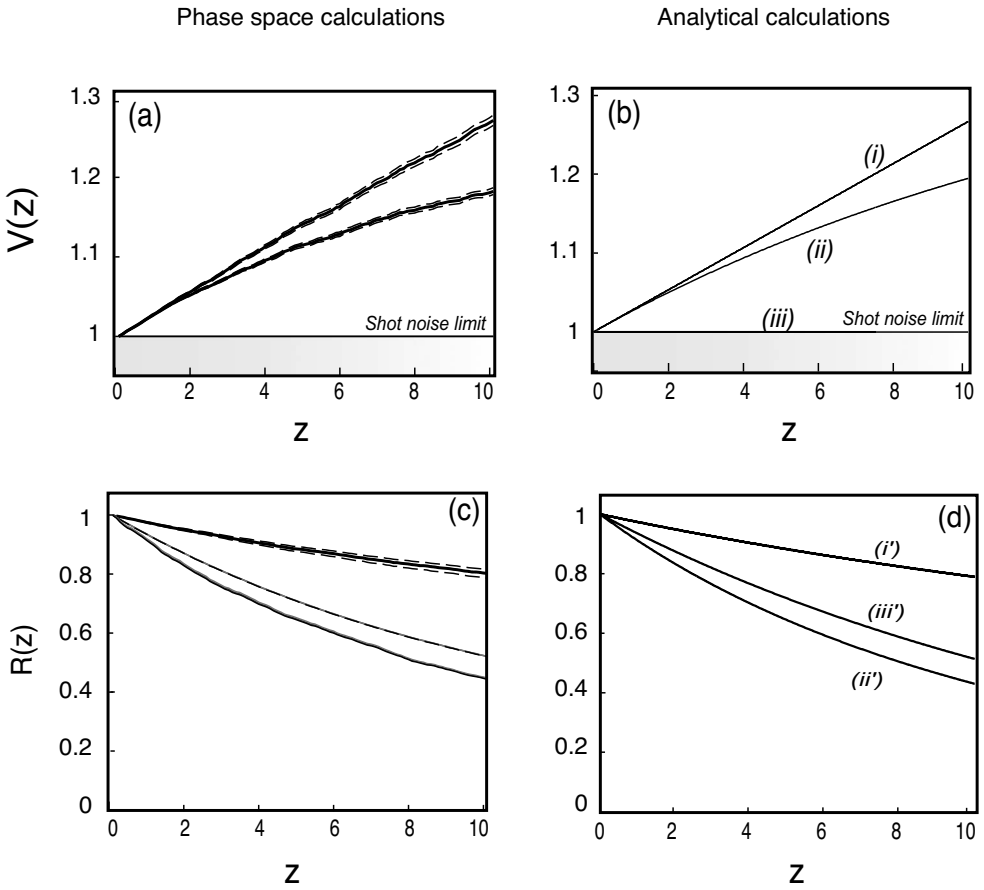

FIG. 3. Signal to noise ratios and noise results for (a) and (c) the numerical solutions and (b) and (d) the analytical solutions. (i) and (i') correspond to $\gamma_c=0.005\gamma$ and $\gamma_0=0$; (ii) and (ii') to $\gamma_c=0.005\gamma$ and $\gamma_0=0.005\gamma$; and (iii) and (iii') to $\gamma_0=0.005\gamma$ and $\gamma_c=0$. The same parameters as for the phase space simulations of light storage of Sec. I A were chosen.

commutation relations. More precisely, it was shown that the output of an ideal linear amplifier with a gain factor $G>1$, relates to the input state by

$$\hat{\mathcal{E}}_{\text{out}} = \sqrt{G}\hat{\mathcal{E}}_{\text{in}} + \sqrt{G-1}\hat{\mathcal{E}}_{\nu}^{\dagger}, \tag{31}$$

where $\hat{\mathcal{E}}_{\nu}^{\dagger}$ is a vacuum mode of the reservoir. The power spectrum at the output of an ideal phase-insensitive amplifier is then given by $S_{\text{out}}^{\pm}=GS_{\text{in}}^{\pm}+G-1$.

We will now follow the approach of Jeffers *et al.* [40] and develop a general theory for amplification and attenuation of a traveling wave. By artificially concatenating m amplifying and attenuating infinitesimal slices with linear amplification $1+a'\delta z$ and attenuation $1-\alpha\delta z$, where $\delta z=z/m$, we will calculate the noise properties of the field using Eq. (31), and compare it with the previous result based on the Heisenberg-Langevin equations. The power spectrum of the field at a slice m can be found to be

$$S_m^{\pm} = \left(1+\frac{(a'-\alpha)z}{m}\right)^m (S_{in}^{\pm}-1)+1 + 2a'\sum_{j=1}^{m}\left(1+\frac{(a'-\alpha)z}{m}\right)^{m-j}. \tag{32}$$

By going to the limit $m\to\infty$ therefore converting the discrete slices into a continuous array, when $\alpha\neq a'$ we get

$$S^{\pm}(z) = \eta'(z)S_{\text{in}}^{\pm} + [1-\eta'(z)](1+N_f'), \tag{33}$$

where

$$N_f' = \frac{2a'}{\alpha-a'} \quad \text{and} \quad \eta'(z) = e^{(a'-\alpha)z}. \tag{34}$$

This general treatment allows us to assess the amount of excess noise present at the output of a system when gain and attenuation are known quantities. Equation (30) can readily be recovered by replacing a' by a and α by $\alpha_0+\alpha_c$ in the EIT system close to zero frequency, which validates this interpretation.

We will now compare the signal to noise ratio and excess noise found by the present theory to the results given by the phase space treatment of Sec. I A in the case of information delay. The signal to noise ratio for both quadratures is defined by

$$\mathcal{R}^{\pm}(z) = \frac{4[\alpha^{\pm}(z)]^2}{V^{\pm}(z)}. \tag{35}$$

Figure 3 shows the evolution of the noise $V(z)=1+V_{\text{noise}}(z)$ and the signal to noise ratio as a function of the depth of propagation in three different situations. We con-

sider the following decoherence combinations: $(\gamma_0,\gamma_c)=(0,0.005\gamma)$, corresponding to curve (i); $(\gamma_0,\gamma_c)=(0.005\gamma,0.005\gamma)$, corresponding to curve (ii); and $(\gamma_0,\gamma_c)=(0.005\gamma,0)$, corresponding to curve (iii). Figures 3(a) and 3(b) are the noise results and Figs. 3(c) and 3(d) are the signal to noise ratio results from the numerical and analytical approaches, respectively.

Both theories are in good agreement. For curve (iii) there is no population exchange between the ground state and therefore the noise never exceeds the shot noise level. For curve (i), the noise increases linearly as predicted when $\gamma_0=0$ whereas for curve (ii), the noise increases exponentially according to Eq. (25).

Figures 3(c) and 3(d) compare the signal to noise ratios results from the two approaches and again a good agreement is found between the numerical simulations and the analytical solutions. Even though the excess noise power is larger for (i) than for (ii) and (iii), the signal transmission is 100% with γ_c only, therefore the output signal to noise ratio is larger for (i') than for (ii') and (iii').

2. Light storage

In this section we present an analytical model of the light storage protocol. Our treatment describes the transfer of information from the modulation sidebands of the probe beam to the atomic coherences in the sample and vice versa, taking into account the same decoherence effects and the finite optical depth.

We will again consider fast switching and symmetric conditions for the writing and retrieval. Information delay can then be seen as light storage where the coupling beam has been switched off and back on immediately afterwards provided the switching of the control beam does not degrade the efficiency or introduce noise. It is clear that during writing and reading the noise can be obtained from the previous delay study. We can therefore ignore the Langevin operators at these stages. However, some care will have to be taken to describe what happens after the switching of the control beam, since, as opposed to information delay, some photons will leak through the medium.

The storage process is treated in three steps. First, we describe the mapping of sidebands of a pulse of duration T to the atomic coherences in momentum space, the writing stage. The second step, the storage time discusses the influence of the decoherences when the coupling beam is off. To show that no noise is introduced by the switching of the coupling beam, the Langevin operators will be retained for this time interval. The last step, the reading stage, is the mapping of the information stored in momentum space back to a probe field. We model the relaxation between the ground states with the decoherence terms γ_0 and γ_c introduced previously, in the same approximate regime (adiabatic elimination of the probe polarization dynamics, and efficient pumping into the dark state). Similarly to Ref. [25], to first order in $\hat{\mathcal{E}}$, two coupled linear equations can be derived and are given by

$$\left(\frac{\partial}{\partial z}+d'/L\right)\hat{\mathcal{E}}(z,t)=\chi\hat{\sigma}_{12}(z,t), \tag{36}$$

$$\left(\frac{\partial}{\partial t}+\Gamma_p\right)\hat{\sigma}_{12}(z,t)=\nu\hat{\mathcal{E}}(z,t), \tag{37}$$

where we introduced the quantities

$$\Gamma_p=\gamma_d+\frac{\Omega_c^2}{(\gamma+\gamma_d/2)},\quad d'=d\frac{\gamma\langle\hat{\sigma}_{11}-\hat{\sigma}_{33}\rangle}{\gamma+\gamma_d/2}. \tag{38}$$

Γ_p describes the pumping rate of photons from the coupling beam and d' the optical depth seen by the probe without coupling beam and in the presence of population shuffling. To simplify the notation we also define

$$\chi=-\frac{gN}{c}\frac{\Omega_c}{\gamma+\gamma_d/2},\quad \nu=-ig\langle\hat{\sigma}_{32}\rangle-\frac{g\Omega_c\langle\hat{\sigma}_{11}-\hat{\sigma}_{33}\rangle}{\gamma+\gamma_d/2}. \tag{39}$$

As these equations are linear, we can deal with the atomic and field variables as c numbers.

Writing stage. We introduce the collective ground-state coherence as the Fourier transform in space of the locally averaged ground-state coherence operator $\sigma_{12}(z,t)$,

$$\sigma_{12}(k,t)=\frac{1}{L}\int_0^L\sigma_{12}(z,t)e^{ikz}dz. \tag{40}$$

After full compression of the probe in the medium this quantity fluctuates with the same standard deviation as the input field as we will show. During the writing stage the state of the probe at each point in space can be found using Eqs. (36) and (37) in the frequency domain. The result is identical to the deterministic part of Eq. (22), as expected. We then obtain the mapping of the field in ω space to the coherences in momentum space when integrating Eq. (37). We consider the memory to work in the linearly dispersive regime, i.e., the differential phase shift seen by all the spectral components of the field is the same. This allows us to change variables from ω_0 to k_0v_g when integrating Eq. (37) and get

$$\sigma_{12}(k,t)=\int dk_0\mathcal{E}_{\text{in}}((k_0-k)v_g)\mathcal{D}_W(k_0,t), \tag{41}$$

where $\mathcal{D}_W$ is a transfer function quantifying the losses due to the finite EIT bandwidth, and the finite length of the cell. Its expression is given in Appendix C. The integration of Eq. (41) is performed between $k-\Delta\omega/(2v_g)$ and $k+\Delta\omega/(2v_g)$.

We now require the frequency where the information is encoded to be smaller than the pumping rate. This condition ensure a high efficiency of the writing process as we will see. In this regime Eq. (41) reduces to

$$\sigma_{12}(k,t)=\frac{\nu v_g}{\Delta\omega\Gamma_p}(1-e^{-\Gamma_p t})\times\int dk_0\mathcal{E}_{\text{in}}[(k_0-k)v_g]\text{sinc}\left(\frac{k_0L}{2}\right). \tag{42}$$

This equation describes a down-sampling of the information from the probe field to the atoms due to a finite optical depth. The information is loaded at a rate Γ_p onto the collective ground-state coherences. This process is much faster than the time it takes for the pulse to enter the sample (which

is on the order of T). When Fourier transforming back to the spatial coordinate at a time $t_{\mathrm{off}} \simeq T$, we get an expression in the form of a convolution

$$\sigma_{12}^{t_{\mathrm{off}}}(z) = \frac{\nu}{\Gamma_p}\mathrm{sinc}(\Delta k z) * [H(L)\mathcal{E}_{\mathrm{in}}(-z/v_g)], \tag{43}$$

where $H(L)$ is a top hat function defining the atomic sample boundaries. For the probe pulse to fit the atomic sample we then require the duration of the pulse to satisfy the relation $T \ll L/v_g$. In this case there is no loss of information, and Eq. (43) can be written

$$\sigma_{12}^{t_{\mathrm{off}}}(z) = \frac{\nu}{\Gamma_p}\mathcal{E}_{\mathrm{in}}(-z/v_g). \tag{44}$$

The statistics of the probe field is then distributed in space onto the atomic ground state as it propagates through the medium, and its energy transferred to the coupling beam.

Storage time. The coupling beam will be switched off at $t=t_{\mathrm{off}}$ and switched back on at a time $t=t_{\mathrm{on}}$. The evolution of the atomic coherence and of the remaining probe field inside the medium will here be solved in this interval.

Because Eq. (21) does not hold in this regime, we now have to consider the spatial dependence of the control beam. From the general ground-state coherence equation of motion in Eq. (17), and the Maxwell equations of the two fields we get

$$\left(\frac{\partial}{\partial t} + \gamma_d\right)\hat{\sigma}_{12}(z,t) = \frac{c}{gN}\frac{\partial}{\partial z}[\hat{\mathcal{E}}(z,t)\Omega_c(z,t)] + \hat{F}_{12}(z,t). \tag{45}$$

As the control beam will be at most on the order of $g\hat{\mathcal{E}}$ after the switching, the first term on the right-hand side is on the order of $g^2\hat{\mathcal{E}}^2/\gamma d$. The effect of those extra photons leaking outside the medium on the ground state coherence is therefore negligible and the writing efficiency of the classical information will not be effected by the switching. This also means that the populations will not change after the switching. The Langevin correlations $\langle \hat{F}_{12}(z,t)\hat{F}_{12}^{\dagger}(z,t)\rangle$ and $\langle \hat{F}_{12}^{\dagger}(z,t)\hat{F}_{12}(z,t)\rangle$ only depend on the populations so their value will not differ significantly from the writing and reading stage. Again, the excess noise can be calculated from the previous delay study. After neglecting those two terms we obtain

$$\sigma_{12}^{t_{\mathrm{on}}}(z) = e^{-\gamma_d(t_{\mathrm{on}}-t_{\mathrm{off}})}\sigma_{12}^{t_{\mathrm{off}}}(z) \tag{46}$$

which describes a simple exponential decay of the coherences over time due to a nonzero dephasing rate γ_d.

Reading stage. To describe the reading stage we evaluate the coherences in the presence of a field on the probe transition in momentum space. We first solve for $\sigma_{12}(k,t)$ independently of the probe field by combining Eqs. (36) and (37). We obtain

$$\sigma_{12}(k,t) = e^{-\beta(k)t}\sigma_{12}^{t_{\mathrm{on}}}(k), \tag{47}$$

where

$$\beta(k) = \Gamma_p - \frac{\nu\chi}{d/L - ik}. \tag{48}$$

We will follow the same procedure as in the writing stage. The Maxwell Eq. (36) is solved in ω space to give

$$\mathcal{E}(z,\omega) = \int d\omega_0 \sigma_{12}^{t_{\mathrm{on}}}\left(\frac{\omega-\omega_0}{v_g}\right)\mathcal{D}_R(z,\omega_0), \tag{49}$$

where $\mathcal{D}_R$ is a transfer function now affecting the transfer from the atomic coherences to the field and is given in Appendix C. The integration of Eq. (49) is performed between $\omega - v_g\Delta k/2$ and $\omega + v_g\Delta k/2$. Under the same condition as for the writing stage (large enough pumping rate Γ_p) we obtain

$$\mathcal{E}(z,\omega) = \frac{\chi L}{v_g \Delta k d'}(1 - e^{-d'z/L}) \times \int d\omega_0 \sigma_{12}^{t_{\mathrm{on}}}\left(\frac{\omega-\omega_0}{v_g}\right)\mathrm{sinc}\left(\frac{\omega_0 T}{2}\right). \tag{50}$$

The down-sampling also occurs when the information is transferred from the ground-state coherences to the probe due to the finite optical depth. We can again transform this expression in time and space to obtain a relation between the field and the atoms at the output of the sample given by

$$\mathcal{E}_{\mathrm{out}}(t) = \frac{\chi L}{d'}\mathrm{sinc}(\Delta\omega t) * [H(T)\sigma_{12}^{t_{\mathrm{on}}}(-v_g t)]. \tag{51}$$

This expression can be simplified further in the case where the retrieved probe fits entirely within the atomic sample, i.e., when the duration of the pulse T satisfies the relation $T \ll L/v_g$. There is then no loss of information and Eq. (51) can be written

$$\mathcal{E}_{\mathrm{out}}(t) = \frac{\chi L}{d'}\sigma_{12}^{t_{\mathrm{on}}}(-v_g t). \tag{52}$$

By continuity arguments one can combine Eqs. (52), (44), and (46) to show that

$$\mathcal{E}_{\mathrm{out}} = \frac{\nu\chi L}{\Gamma_p d'}e^{-\gamma_d(t_{\mathrm{on}}-t_{\mathrm{off}})}\mathcal{E}_{\mathrm{in}}. \tag{53}$$

This expression relates the input and output probe states in the presence of pure dephasing and population exchange between the ground states in the limit of large density and large pumping rate Γ_p. One can show that when $\gamma_d = 0$, the output is then the perfect replica of the input state.

The upper bound for T has to be satisfied for the pulse to fit the atomic sample. With a long input pulse, $\Delta\omega$, a high density or a weak coupling beam is required, whereas for a short input pulse v_g/L can be made larger. On the other hand, the upper bound for $\Delta\omega$ defines the minimum EIT bandwidth tolerable to minimize the losses. A short input pulse will require a large coupling beam power, whereas a weaker coupling beam power (narrower EIT bandwidth) can be used with a longer pulse. The time-bandwidth product of the system $(\Gamma_p L/v_g)$ is d', i.e., the number of independent samples from the probe that can be faithfully stored depends only on the density. At infinite density one can then store an infinitely broad probe spectrum. We see that not only does γ_c introduce

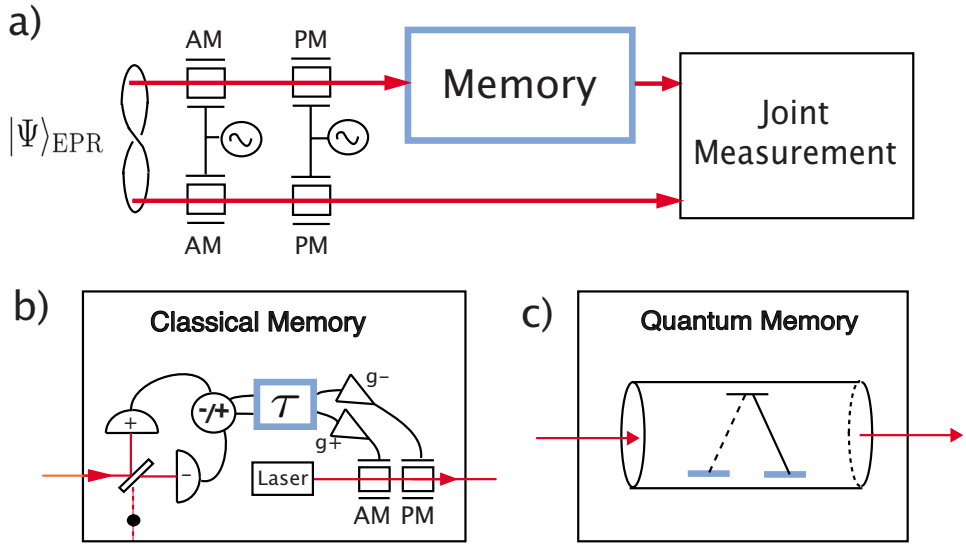

FIG. 4. (Color online) (a) General schematics for characterizing an optical memory. A pair of EPR entangled beams are encoded with amplitude and phase quadrature information. One of these beams is injected into, stored, and readout from the optical memory while the other is being propagated in free space. A joint measurement with appropriate delay is then used to measure the quantum correlations between the quadratures of the two beams. (b) A classical teleporter scheme used as an optical memory. The input state is measured jointly on both quadratures using two homodyne detection schemes. Analogous to classical teleportation the measured information is stored for time τ before fed-forward onto an independent laser beam with a feed-forward gain, g. The feed-forward gain is analogous to a transmission of $\sqrt{\eta(\omega)}$ for EIT-based memories. (c) Quantum memory using EIT. The input state is stored in the long lived ground state coherence of three level atoms in a Λ configuration.

excess noise on the output probe mode as discussed in the previous sections, but it also reduces the time bandwidth product at a given d.

This result is similar to the one found in the general case of time varying coupling beam in Ref. [13]. With a coupling power calculated by equating the length of the pulse in the cell with the length of the cell $\Omega_c^2 = d\gamma/T$, the condition $Td\gamma \gg 1$ is obtained. Our condition requires the full width at half maximum of the pulse to be smaller than the cell length. As also mentioned in Ref. [13], the input and output pulse durations (which are identical in our case) also have to satisfy the relation $T\gamma_d \ll 1$ for the information to be imprinted onto the atoms before the pulse is absorbed. We note that provided Eq. (54) holds, the condition $\frac{\Omega^2}{\gamma\gamma_d} \gg d$ is sufficient for $T\gamma_d \ll 1$ to hold. As already mentioned, this is the case in all the numerical simulations and analytical derivations presented in this paper.

II. QUANTUM INFORMATION BENCHMARKS

In this section we will investigate the storage of optical information from a quantum information perspective. We will benchmark the results obtained in our modeling against known quantum information criteria. These criteria, which are fidelity, signal transfer coefficients and conditional variances, will enable the determination of whether a quantum strategy has been used in the storage and readout of a quantum state; whether an EIT-based quantum memory is possible in an experimentally realistic situation, and whether the output of the storage process is indeed the best clone of its input.

Figure 4 shows the schematics of our quantum memory benchmark. It was shown in Ref. [41] that the optimal classical measure and prepare strategy for optical memory is the classical teleporter scheme as shown in Fig. 4(b), and we therefore benchmark the performance of our EIT quantum memory against this setup. In this classical scheme, the storage time can be arbitrarily long without additional degradation. However, two conjugate observables cannot be simultaneously measured and stored without paying a quantum of duty [21,42]. Moreover, the encoding of information onto an independent beam using amplitude and phase modulators will also introduce another quantum of noise. In total, the entire process will incur an additional two quanta of noise onto the output optical state.

Possibly the best known benchmark in quantum information protocols is the fidelity which measures the wave function overlap between the output and input states. It is given by

$$\mathcal{F} = \langle \Psi_{\text{in}} | \hat{\rho}_{\text{out}} | \Psi_{\text{in}} \rangle, \tag{54}$$

which, in the Wigner representation, can be written

$$\mathcal{F} = 2\pi \int \int W_{\text{in}}(X^+, X^-) W_{\text{out}}(X^+, X^-) dX^+ dX^-. \tag{55}$$

For Gaussian states with coherent amplitude $\alpha^{\pm}$ and power spectrum $S^{\pm}$, the Wigner function is

$$\mathrm{W}(X^+, X^-) = \frac{2}{\pi S^+ S^-} e^{-(X^+ - 2\alpha^+)^2/2S^+ - (X^- - 2\alpha^-)^2/2S^-}. \tag{56}$$

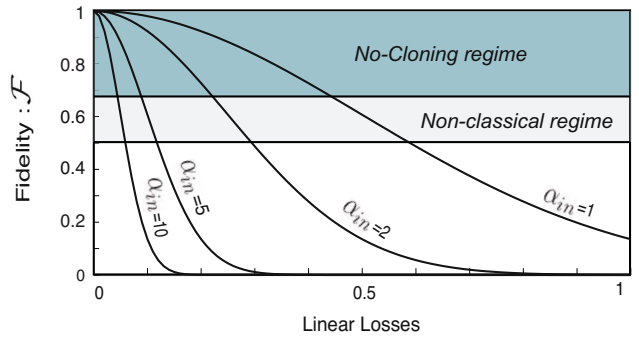

FIG. 5. (Color online) Fidelity as a function of memory loss for EIT for $\alpha_{\text{in}}(\omega)=10,5,2,1$. The nonclassical and no-cloning regimes are reached when $\mathcal{F}\geq 1/2$ and $\mathcal{F}\geq 2/3$, respectively, for large input state amplitudes.

The fidelity of the classical teleporter scheme can be easily calculated [23] using Eqs. (56) and (57) and gives

$$\mathcal{F}=\frac{2e^{-k^{+}-k^{-}}}{\sqrt{(2+V_{\text{noise}}^{+})(2+V_{\text{noise}}^{-})}}, \tag{57}$$

where $k^{\pm}=\alpha_{\text{in}}^{\pm}(1-g^{\pm})^2/(2+V_{\text{noise}}^{\pm})$, $V_{\text{noise}}^{\pm}$ are the noise variances of the output field for the amplitude and phase quadratures and $g^{\pm}$ is the feed-forward gain. For an ideal classical memory with unity gain, $g^{\pm}=1$, one can see from the previous argument that a coherent input state will give $V_{\text{noise}}^{\pm}=2$, thus giving a classical limit of $\mathcal{F}\geq 0.5$. It has been shown by Grosshans and Grangier [43] that when the fidelity of a teleporter $\mathcal{F}\geq 2/3$, the output state is guaranteed to be the best cloned copy of the input state. This fidelity limit called the no-cloning limit for teleportation corresponds to the addition of only one quantum of noise in the entire process.

The use of entanglement in the context of quantum teleportation, or for example EIT for quantum memories is necessary to break these limits. We now quantify EIT-based quantum memories using this criterion. There is a direct analogy between the feed-forward gain g and the EIT transmission $\sqrt{\eta(\omega)}$. Figure 5 shows the behavior of $\mathcal{F}$, as defined in Eq. (58) using $g=\sqrt{\eta(\omega)}$, with varying memory loss for different coherent state amplitudes. This shows that fidelity is a state-dependent measure.

The formula for the fidelity can be extended to mixed input states using

$$\mathcal{F}=[\text{tr}(\sqrt{\sqrt{\hat{\rho}_{\text{in}}}\hat{\rho}_{\text{out}}\sqrt{\hat{\rho}_{\text{in}}}})]^2. \tag{58}$$

Jeong *et al.* [44] showed that this formula can again be used to benchmark quantum information protocols. Nevertheless, characterizing quantum memory using the state-dependent fidelity as a measure will be complicated for exotic mixed states.

An alternative measure to fidelity for the characterization of quantum information protocols was proposed by Grangier *et al.* [45] for quantum nondemolition measurement and by Ralph and Lam [21] for quantum teleportation. This alternative uses the signal transfer coefficients $T^{\pm}$ and the input-output conditional variances $V_{\text{CV}}^{\pm}$ to establish the efficacy of a process. The conditional variances and signal transfer coefficients are defined as

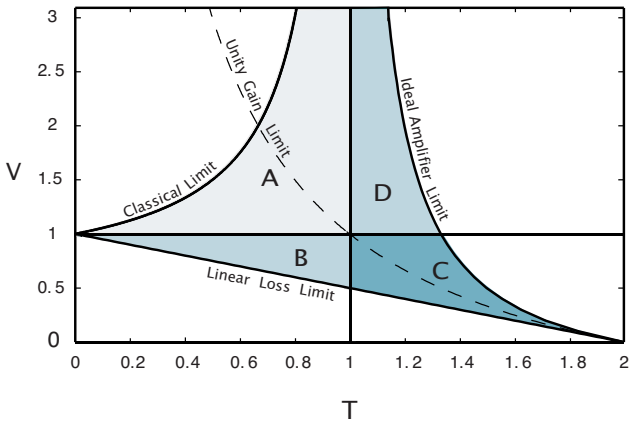

FIG. 6. (Color online) Diagram for total signal transfer coefficient T versus conditional variance product V. The classical limit line shows the optimal performance of a classical teleporter. The linear loss limit defines the performance of an EIT-based memory that does not produce excess noise. The unity gain curve is obtained with increasing excess noise in an EIT system with no loss. Regions A, B, C, and D correspond to the quantum regime; regions B and C represent the regime where EPR entanglement is preserved; region D is the lossless amplification region; region C denotes the no-cloning limit.

$$V_{\text{CV}}^{\pm}=V_{\text{out}}^{\pm}-\frac{|\langle\hat{X}_{\text{in}}^{\pm}\hat{X}_{\text{out}}^{\pm}\rangle|^2}{V_{\text{in}}^{\pm}}, \tag{59}$$

$$T^{\pm}=\frac{\mathcal{R}_{\text{out}}^{\pm}}{\mathcal{R}_{\text{in}}^{\pm}}, \tag{60}$$

where $\mathcal{R}_{\text{out/in}}^{\pm}$ is the signal to noise ratio of the output/input field defined by

$$\mathcal{R}_{\text{in/out}}^{\pm}=\frac{4(\alpha_{\text{in/out}}^{\pm})^2}{V_{\text{in/out}}^{\pm}}. \tag{61}$$

We now define two parameters that take into account the performances of the system on both conjugate observables

$$V=\sqrt{V_{\text{CV}}^{+}V_{\text{CV}}^{-}}, \tag{62}$$

$$T=T^{+}+T^{-}. \tag{63}$$

Figure 6 shows the plot of a TV diagram. Similar to the fidelity, there are corresponding classical and no-cloning limits in the TV diagram for a teleporter or an optical memory. It can be shown that a classical teleporter cannot overcome the $T>1$ or $V<1$ limits. By tuning the feed-forward gain g a classical teleporter will perform at best at the "classical limit" curve as shown in Fig. 6. Reference [21] shows that this classical limit can be surpassed using quantum resource (region A). With limited quantum resource, it is possible to have an output state with $V<1$ (region B) or $T>1$ (region D). When the input state is from a pair of entangled beams,

this performance corresponds to the preservation of Einstein-Podolsky-Rosen (EPR) entanglement at the output [46]. With a stronger quantum resource, $T>1$ and $V<1$ can be satisfied simultaneously. Grosshans and Grangier [43] showed that under these conditions the output state represents the best cloned copy of the input. The lower right quadrant of the *TV* diagram (region C) therefore corresponds to the no-cloning regime.

We now characterize the EIT-based quantum memory in terms of the *TV* diagram. When an EIT system does not generate excess noise, the performance of the memory is described by the linear loss limit line. Assuming that the transmission through the EIT medium is identical for both quadratures, it can be shown that $V=1-\eta(\omega)$ and $T=2\eta(\omega)$. We note that the result suggests that an EIT with linear loss will surpass the classical limit independent of $\sqrt{\eta(\omega)}$. This is because unlike the classical teleporter, the output state obtained from a linear loss EIT is not being measured throughout the transmission. Thus there is no measurement quantum duty for all transmittivities. Moreover, an input entangled state through a linear loss device will always preserve some entanglement at the output.

However, when excess noise is introduced in the storage process, T will decrease and V increase more rapidly. This is the case if for example some phase insensitive amplification is involved. Indeed we have seen in the previous section that $G-1$ quanta of noise will be introduced for a lossless memory with a gain G in order to preserve the commutation relations of the optical field at the output. The performance of such a lossless and amplifying memory is then described by the ideal lossless amplifier line on the *TV* diagram where one can show that $V=G-1$ and $T=2G/(2G-1)$. The optimum situation will be when the gain of the amplifier is unity, so that $T=2$ and $V=0$. As the gain increases the memory no longer performs in the no-cloning regime and reaches region *D*, where no quantum correlation exists between the input and output states anymore, even though the signal transfer is always larger than what a classical memory could achieve.

There are other possible sources of noise that do not amplify the signal. For example, any transfer between the coupling beam and the probe via nonlinear processes [47] or nonideal polarizers will contribute to excess noise. We can introduce the excess noise phenomenologically with V_{noise}, which we can assume to be quadrature independent. The *TV* performance is now given by $V=1-\eta(\omega)+V_{\text{noise}}$ and $T=2\eta(\omega)/(1+V_{\text{noise}})$. Unlike classical teleportation and in the absence of an amplification process, $\sqrt{\eta(\omega)}$ can only be less than or equal to unity. If we assume perfect transmittivity with $\sqrt{\eta(\omega)}=1$, increasing excess noise produces the unity gain curve, or unity classical transmission curve in the *TV* diagram. We note that although the classical input signal is perfectly transmitted, the excess noise leads to a degradation on both T and V.

We will now define the parameters required to reach the quantum regime in the case when the noise arises from amplification and when its origin is not related to any gain in the medium separately. We plot these quantum regimes with excess noise versus linear loss in Fig. 7(a), and memory gain versus loss in Fig. 7(b). In particular, to define the graph

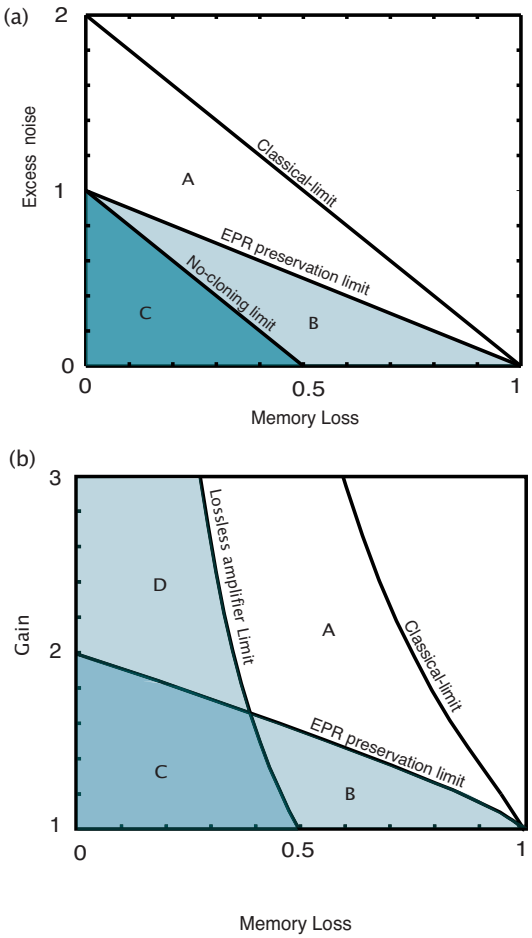

FIG. 7. (Color online) Classical, EPR and no-cloning regimes plotted as a function of EIT linear loss and excess noise in (a). A is the nonclassical regime, B is the EPR regime, and C is the no-cloning regime. These limits are drawn in (b) on a loss-gain plot and have been derived from Eq. (33). Contrary to the case of (a), with a large enough gain and sufficiently low losses in the memory, region (d) can be reached.

shown Fig. 7(b), we calculated T and V using our theory for amplification and attenuation with Eq. (33). Then, we found the linear gain and linear losses for which the EIT performance crosses our benchmarks. The gain (loss) term in Fig. 7 is the total amplification (attenuation) introduced by the memory defined as e^{-al} and e^{al}, respectively. For example, with no population exchange between ground states in EIT, the gain is 1. These diagrams determine whether an experiment is sufficiently low noise and transmissive for quantum information storage. The no-cloning limit can only be surpassed when $\sqrt{\eta(\omega)}>0.5$ and $V_{\text{noise}}<1$ simultaneously in both cases. We note that similar figure of merit has recently been developed by Coudreau *et al.* [48], during the course of this work.

Using the numerical model presented in Sec. I A, we investigate the parameters required to implement the storage of optical information in the quantum regime. We model the situation where a medium of length $L=12$ cm with an atomic density of 10^{12} cm^3 is used to store an optical signal encoded on a pulse. The length of the pulse is chosen here to

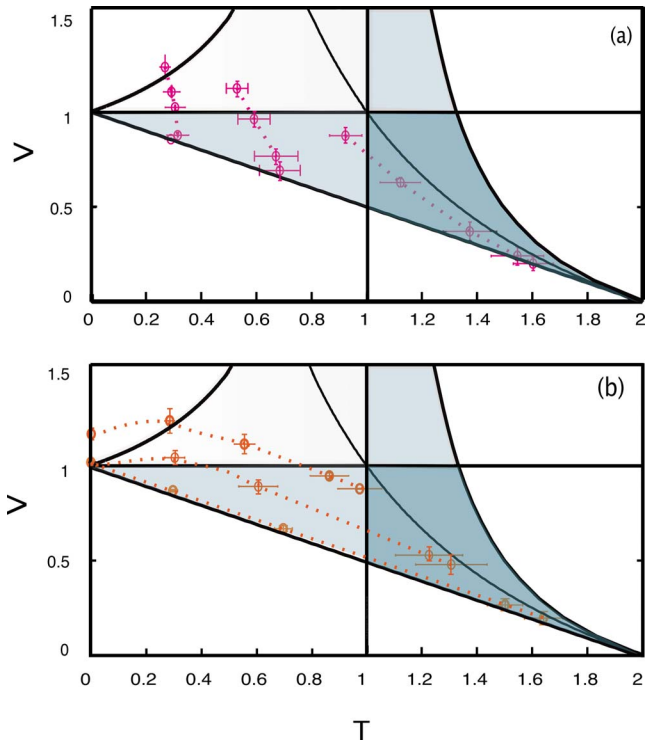

FIG. 8. (Color online) *TV* diagrams showing the performance of the EIT memory. (a) The evolution of its efficiency for three different γ_0 values, the dotted lines representing the loci for a constant γ_0 and varying γ_c. (b) The evolution the EIT memory for three different γ_c values, the dotted lines representing the loci for a constant γ_c and varying γ_0.

be $50/\gamma$ and the information is encoded on the quadrature amplitudes at a sideband frequency $\omega=0.005\gamma$. We plot the evolution of the EIT performance as a function of the decoherence rates in Fig. 8. At zero decoherence rates, we note that (T,V) is not (2,0) because of the finite optical thickness of the EIT medium. With the above parameters the bounds in Eq. (54) are satisfied by only one order of magnitude which makes the storage process nonideal even in the absence of dephasing. The no-cloning limit is, however, still beaten in that case. We see that the evolution of the performances of the memory with γ_0 and γ_c is radically different as predicted earlier. In both cases, when the decoherence rates increase, T monotonically decreases and at some decoherence rate value the quantum regime is no longer reached, but an increase in γ_c results in a faster increase of the condition variance, as expected. It is also important to note that for any value of the couple (γ_0,γ_c) the region D is never reached, this is because the gain term from population exchange is always associated with loss so the EIT memory never gets within the lossless amplifier regime.

We also wish to stress the difference between our figure of merit and the one used in Ref. [13]. The present work considers the signal to noise ratios for both quadratures at a given sideband frequency, as well as the amount of excess noise added to the field. The ratio between the total number of photons between the output and input also provides a figure of merit for a quantum memory that does not introduce uncorrelated extra photons in the light field output mode.

III. CONCLUSION

We have developed a quantum multi-mode treatment describing the storage of the quantum information encoded on the sideband quadrature amplitudes of a light pulse using both stochastic simulations and an analytical treatment for EIT. The two models included the atomic noise and decoherence rates of realistic experiments. In our model we have, however, assumed an ideal three level atomic structure with incident light fields that have constant transverse spatial intensities. Transverse mode effects might have important consequences on the efficiency of the memory, but are hard to model accurately [49,50]. We also assumed a monokinetic atomic ensemble for which light is exactly tuned on resonance and also neglected the effect of the back coupling from spontaneous emission into the light field, such as "radiation trapping" [51]. With these assumptions, the optimum sideband frequency for which the storage process can be efficiently performed depends mainly on the optical density and the coupling beam power chosen to set up the EIT. We have also calculated the time-bandwidth product of the EIT memory and have shown that it only depends on the atomic density.

We finally proposed the use of quantum information criteria to benchmark the performance of quantum memories against an optimal classical measure-and-prepare scheme. We have shown that for typical decoherence rates in current experiments quantum information on the sideband quadrature amplitudes can be stored for milliseconds in the no-cloning regime, in the presence of small amounts of linear loss and excess noise.

ACKNOWLEDGMENTS

We thank O. Glöckl, M. T. L. Hsu, B. C. Buchler, J. J. Longdell, and H.-A. Bachor for useful discussions. We would also like to thank the anonymous referee for enlightening comments. We acknowledge financial support from the Australian Research Council Centre of Excellence scheme.

APPENDIX A

We list here the stochastic equations describing the evolution of the atomic c numbers in the presence of a quantized probe field and a classical pump for one slice δz of the medium. The c numbers α and β represent the operators $\hat{\mathcal{E}}^{\dagger}(z,t)$ and $\hat{\mathcal{E}}(z,t)$. The atomic variables $(\sigma_3,\sigma_4,\sigma_5,\sigma_6,\sigma_7,\sigma_9,\sigma_{10},\sigma_{11})$ represent the operators $(\hat{\sigma}_{13},\hat{\sigma}_{23},\hat{\sigma}_{12},\hat{\sigma}_{11},\hat{\sigma}_{22},\hat{\sigma}_{21},\hat{\sigma}_{32},\hat{\sigma}_{31})$. The equation for σ_8 linearly depends on σ_6 and σ_7 via the population preservation equation $\sigma_6+\sigma_7+\sigma_8=1$ and is therefore not computed. The noise terms n_j (for $j=1$ to 18) are all δ correlated and follow a Gaussian distribution, and have been normalized by $\frac{1}{\sqrt{n\mathcal{A}}}$. The variables $\bar{g}$, $\bar{\gamma}_0$, $\bar{\gamma}_c$, and $\bar{E}_c$ are all normalized to the spontaneous emission rate γ:

$$\dot{\sigma}_3 = -(1+\bar{\gamma}_0/2+\bar{\gamma}_c/2)\sigma_3 + \bar{E}_c\sigma_5 - \alpha(1-2\sigma_6-\sigma_7) + \sqrt{\frac{\bar{g}}{2\gamma}}(\alpha/\bar{g}-\sigma_3)n_1 + i\sqrt{\frac{\bar{g}}{2\gamma}}(\alpha/\bar{g}+\sigma_3)n_2 - (\alpha\sigma_4+\bar{E}_c\sigma_3)(n_3-in_4)$$
$$+\frac{1}{2\sqrt{\gamma}}\sqrt{(\bar{\gamma}_c+\bar{\gamma}_0/2)(1-\sigma_7-\sigma_6)}(in_7+\sqrt{2}n_{10}+in_{12}) + \sqrt{2}(\bar{\gamma}_c+\bar{\gamma}_0/2)\sigma_4(n_{14}-in_{13}),$$

$$\dot{\sigma}_4 = -(1+\bar{\gamma}_0/2+\bar{\gamma}_c/2)\sigma_4 + \alpha\sigma_9 + \bar{E}_c(\sigma_6+2\sigma_7-1) + \sqrt{\frac{\bar{g}}{2\gamma}}(\sigma_4-\bar{E}_c/\bar{g})n_1 - i\sqrt{\frac{\bar{g}}{2\gamma}}(\sigma_4+\bar{E}_c/\bar{g})n_2$$
$$+(n_3+in_4)/\gamma + (\bar{\gamma}_c+\bar{\gamma}_0/2)(1-\sigma_6-\sigma_7)(in_{15}+n_{16})/4,$$

$$\dot{\sigma}_5 = -(\bar{\gamma}_c+\overline{\gamma_0})\sigma_5 - \alpha\sigma_{10} - \bar{E}_c\sigma_3 - \sqrt{\frac{\bar{g}}{2\gamma}}\sigma_5(n_1-in_2) + [\alpha(\sigma_6-\sigma_7)+(\bar{\gamma}_c+\bar{\gamma}_0/2)\sigma_3](n_3-in_4)/2 + \frac{1}{2\sqrt{2}\gamma}(n_5-in_6)$$
$$+\frac{1}{2\sqrt{\gamma}}\sqrt{\alpha\sigma_{11}+\beta\sigma_3+1-\sigma_6-\sigma_7+2\bar{\gamma}_0\sigma_7+\bar{\gamma}_c(\sigma_6+\sigma_7)}(in_8+\sqrt{2}n_9+in_{11}),$$

$$\dot{\sigma}_6 = 1-\sigma_6-\sigma_7-\bar{\gamma}_c(\sigma_6-\sigma_7) - \alpha\sigma_{11} - \beta\sigma_3 - \frac{\bar{\gamma}_c}{\sqrt{2\bar{g}\gamma}}(n_1+in_2) - \alpha\sigma_9(n_3-in_4)/2$$
$$+\sqrt{\alpha\sigma_{11}+\beta\sigma_3+1-\sigma_6-\sigma_7}\sqrt{\alpha\sigma_{11}+\beta\sigma_3+1-\sigma_6-\sigma_7+2\bar{\gamma}_0\sigma_7+\bar{\gamma}_c(\sigma_6+\sigma_7)}(n_5+in_6) + \sqrt{\frac{\bar{\gamma}_c}{2\gamma}(\sigma_6+\sigma_7)}(n_7-n_{12})$$
$$-\frac{1}{\sqrt{\gamma}}\sqrt{\alpha\sigma_{11}+\beta\sigma_3+1-\sigma_6-\sigma_7}n_9 + \sqrt{\alpha\sigma_{11}+\beta\sigma_3+1-\sigma_6-\sigma_7}\sqrt{\alpha\sigma_{11}+\beta\sigma_3+1-\sigma_6-\sigma_7+\bar{\gamma}_c(\sigma_6+\sigma_7)+\bar{\gamma}_0\sigma_7}(n_{14}-in_{13})$$
$$-\beta\sigma_5(in_{15}+n_{16})/2 - \frac{\bar{\gamma}_c}{\gamma}(n_{18}-in_{17}),$$

$$\dot{\sigma}_7 = 1-\sigma_6-\sigma_7-\bar{\gamma}_c(\sigma_7-\sigma_6) - \bar{E}_c(\sigma_4+\sigma_{10}) + \frac{\bar{\gamma}_c}{\sqrt{2\bar{g}\gamma}}(n_1+in_2) + \alpha\sigma_9(n_3-in_4)/2 + \sqrt{2}(\alpha\sigma_{10}+\bar{E}_c\sigma_3)(n_5+in_6) + \sqrt{\frac{\bar{\gamma}_c}{2\gamma}(\sigma_6+\sigma_7)}$$
$$\times(n_{12}-n_7) + \frac{1}{\sqrt{2}\gamma}\sqrt{\bar{E}_c(\sigma_4+\sigma_{10})+1-\sigma_6-\sigma_7}(n_8-n_{11}) + \sqrt{2}(\beta\sigma_4+\bar{E}_c\sigma_{11})(n_{14}-in_{13}) + \beta\sigma_5(n_{16}+in_{15})/2 + \frac{\bar{\gamma}_c}{\sqrt{2\bar{g}\gamma}}(n_{18}$$
$$-in_{17}),$$

$$\dot{\sigma}_9 = -(\bar{\gamma}_c+\bar{\gamma}_0)\sigma_9 - \beta\sigma_4 - \bar{E}_c\sigma_{11} + \frac{1}{2\sqrt{\gamma}}\sqrt{\alpha\sigma_{11}+\beta\sigma_3+1-\sigma_6-\sigma_7+\bar{\gamma}_c(\sigma_6+\sigma_7)+2\bar{\gamma}_0\sigma_7}(-in_8+\sqrt{2}n_9-in_{11}) + \frac{1}{2\sqrt{2}\gamma}(n_{14}$$
$$+in_{13}) + [\beta(\sigma_6-\sigma_7)+(\bar{\gamma}_c+\bar{\gamma}_0/2)\sigma_{11}](in_{15}+n_{16})/2 - \sqrt{\frac{\bar{g}}{2\gamma}}\sigma_9(in_{17}+n_{18}),$$

$$\dot{\sigma}_{10} = -(1+\bar{\gamma}_0/2+\bar{\gamma}_c/2)\sigma_{10} + \beta\sigma_5 + \bar{E}_c(2\sigma_7+\sigma_6-1) + (\bar{\gamma}_c+\bar{\gamma}_0/2)(1-\sigma_6-\sigma_7)(n_3-in_4)/4 + (n_{16}-in_{15})/\gamma + i\sqrt{\frac{\bar{g}}{2\gamma}}(\sigma_{10}$$
$$+\bar{E}_c/\bar{g})n_{17} + \sqrt{\frac{\bar{g}}{2\gamma}}(\sigma_{10}-\bar{E}_c/\bar{g})n_{18},$$

$$\dot{\sigma}_{11} = -(1+\bar{\gamma}_0/2+\bar{\gamma}_c/2)\sigma_{11} + \bar{E}_c\sigma_9 - \beta(1-2\sigma_6-\sigma_7) + \sqrt{2}(\bar{\gamma}_0/2+\bar{\gamma}_c)\sigma_{10}(n_5+in_6) + \frac{1}{2\sqrt{\gamma}}\sqrt{(\bar{\gamma}_c+\bar{\gamma}_0/2)(1-\sigma_6-\sigma_7)}(-in_7$$
$$+\sqrt{2}n_{10}-in_{12}) - (\beta\sigma_{10}+\bar{E}_c\sigma_{11})(in_{15}+n_{16}) - i\sqrt{\frac{\bar{g}}{2\gamma}}(\beta/\bar{g}+\sigma_{11})n_{17} + \sqrt{\frac{\bar{g}}{2\gamma}}(\beta/\bar{g}-\sigma_{11})n_{18}. \quad \text{(A1)}$$

The Stratonovitch corrections to the Ito-SDE $(\partial_t\sigma_3, \partial_t\sigma_4, \partial_t\sigma_5, \partial_t\sigma_6, \partial_t\sigma_7, \partial_t\sigma_9, \partial_t\sigma_{10}, \partial_t\sigma_{11})$ are

$$\left(\frac{3\alpha}{2\gamma},\frac{\bar{E}_c}{2\gamma},\frac{(\bar{\gamma}_c-1)\sqrt{1-\alpha_6-\alpha_7+\alpha\sigma_{11}+\beta\sigma_3}}{4\gamma\sqrt{2}\sqrt{1-(1-\bar{\gamma}_c\alpha_6-(1-\bar{\gamma}_c-\bar{\gamma}_0)\alpha_7+\alpha\sigma_{11}+\beta\sigma_3}},\frac{1}{4\gamma},\frac{1}{4\gamma},\right.$$
$$\left.\frac{(\bar{\gamma}_c-1)\sqrt{1-\alpha_6-\alpha_7+\alpha\sigma_{11}+\beta\sigma_3}}{4\gamma\sqrt{2}\sqrt{1-(1-\bar{\gamma}_c)\alpha_6-(1-\bar{\gamma}_c-\bar{\gamma}_0)\alpha_7+\alpha\sigma_{11}+\beta\sigma_3}},\frac{\bar{E}_c}{2\gamma},\frac{3\beta}{2\gamma}\right). \tag{A2}$$

They are negligibly small compared to the other variables of the Ito-SDE equations and are not used in the simulations.

APPENDIX B

In this Appendix, we list the nonzero Langevin correlations corresponding to the system of Eqs. (17).

$$\langle\tilde{F}_{13}(z_1,\omega_1)\tilde{F}_{13}^{\dagger}(z_2,\omega_2)\rangle=\frac{\delta(z_1-z_2)\delta(\omega_1+\omega_2)}{n\mathcal{A}}\times[(\gamma+\gamma_c+\gamma_0)\langle\hat{\sigma}_{33}\rangle+2\gamma\langle\hat{\sigma}_{11}\rangle-\gamma_c\langle\hat{\sigma}_{11}-\hat{\sigma}_{22}\rangle],$$

$$\langle\tilde{F}_{13}^{\dagger}(z_1,\omega_1)\tilde{F}_{13}(z_2,\omega_2)\rangle=\frac{\delta(z_1-z_2)\delta(\omega_1+\omega_2)}{n\mathcal{A}}\times[2\gamma\langle\hat{\sigma}_{33}\rangle-2(\gamma+\gamma_0+\gamma_c)\langle\hat{\sigma}_{33}\rangle],$$

$$\langle\tilde{F}_{13}^{\dagger}(z_1,\omega_1)\tilde{F}_{12}(z_2,\omega_2)\rangle=\frac{\delta(z_1-z_2)\delta(\omega_1+\omega_2)}{n\mathcal{A}}\times(\gamma_c+\gamma_0)\langle\hat{\sigma}_{32}\rangle,$$

$$\langle\tilde{F}_{12}^{\dagger}(z_1,\omega_1)\tilde{F}_{13}(z_2,\omega_2)\rangle=\frac{\delta(z_1-z_2)\delta(\omega_1+\omega_2)}{n\mathcal{A}}\times(\gamma_c+\gamma_0)\langle\hat{\sigma}_{23}\rangle,$$

$$\langle\tilde{F}_{12}(z_1,\omega_1)\tilde{F}_{12}^{\dagger}(z_2,\omega_2)\rangle=\frac{\delta(z_1-z_2)\delta(\omega_1+\omega_2)}{n\mathcal{A}}\times[(\gamma+\gamma_c+\gamma_0)\langle\hat{\sigma}_{33}\rangle+\gamma_c\langle\hat{\sigma}_{22}+\hat{\sigma}_{11}\rangle+2\gamma_0\langle\sigma_{11}\rangle],$$

$$\langle\tilde{F}_{12}^{\dagger}(z_1,\omega_1)\tilde{F}_{12}(z_2,\omega_2)\rangle=\frac{\delta(z_1-z_2)\delta(\omega_1+\omega_2)}{n\mathcal{A}}\times(\gamma\langle\hat{\sigma}_{33}\rangle+\gamma_c\langle\hat{\sigma}_{22}+\hat{\sigma}_{11}\rangle+2\gamma_0\langle\sigma_{22}\rangle). \tag{B1}$$

APPENDIX C

In this appendix we give the transfer function quantifying the losses and phase shifts introduced during the writing and reading stages. In the presence of both pure dephasing and population shuffling, the state of the atoms is given by Eq. (41), where the transfer function $\mathcal{D}_W(k_0,t)$ is

$$\mathcal{D}_W(k_0,t)=\frac{\nu v_g}{\Delta\omega}\left(\frac{e^{\{ik_0-\zeta((k-k_0)v_g)\}L}-1}{ik_0L-\zeta((k-k_0)v_g)L}\right)\times\left(\frac{e^{[\Gamma_p-i(k-k_0)v_g]t}-1}{\Gamma_p-i(k-k_0)v_g}\right), \tag{C1}$$

where $\zeta(\omega)=\mathrm{Re}[\Lambda(\omega)]$.

The state of the light field during the recall stage is given by Eq. (49) where the transfer function $\mathcal{D}_R(z,\omega_0)$ is

$$\mathcal{D}_R(z,\omega_0)=\frac{\chi}{\Delta k v_g}\left(\frac{e^{[i\omega_0-\zeta'((\omega-\omega_0)/v_g)]t}-1}{\left[i\omega_0-\zeta'\left(\frac{\omega-\omega_0}{v_g}\right)\right]T}\right)\times\left(\frac{e^{(d'/L-i(\omega-\omega_0)/v_g)z}-1}{d'-i\frac{\omega-\omega_0}{v_g}L}\right), \tag{C2}$$

where $\zeta'(k)=\mathrm{Re}[\beta(k)]$. Those transfer functions account for all the physics involved during the storage process when the control beam is constant in time, with ground decoherence rates and finite atomic density.

[1] A. E. Kozhekin, K. Molmer, and E. Polzik, Phys. Rev. A **62**, 033809 (2000).
[2] B. Julsgaard, J. Sherson, J. I. Cirac, J. Fiurasek, and E. S. Polzik, Nature (London) **432**, 482 (2004).
[3] S. A. Moiseev and S. Kroll, Phys. Rev. Lett. **87**, 173601 (2001).
[4] N. Sangouard, C. Simon, M. Afzelius, and N. Gisin, Phys. Rev. A **75**, 032327 (2007).

[5] G. Hétet, J. J. Longdell, A. L. Alexander, P. K. Lam, and M. J. Sellars, Phys. Rev. Lett. **100**, 023601 (2008).
[6] C. Liu, Z. Dutton, C. H. Behroozi, and L. V. Hau, Nature (London) **409**, 490 (2001).
[7] M. Fleischhauer and M. D. Lukin, Phys. Rev. Lett. **84**, 5094 (2000).
[8] D. F. Phillips, A. Fleischhauer, A. Mair, R. L. Walsworth, and M. D. Lukin, Phys. Rev. Lett. **86**, 783 (2001).
[9] J. J. Longdell, E. Fraval, M. J. Sellars, and N. B. Manson, Phys. Rev. Lett. **95**, 063601 (2005).
[10] T. Chanelière, D. N. Matsukevich, S. D. Jenkins, S.-Y. Lan, T. A. B. Kennedy, and A. Kuzmich, Nature (London) **438**, 833 (2005).
[11] J. Laurat, H. de Riedmatten, D. Felinto, C. W. Chou, E. W. Schomburg, and H. J. Kimble, Opt. Express **14**, 6912 (2006).
[12] M. D. Eisaman, A. André, F. Massou, M. Fleischhauer, A. S. Zibrov, and M. D. Lukin, Nature (London) **438**, 837 (2005).
[13] A. V. Gorshkov, A. André, M. Fleischhauer, A. S. Sorensen, and M. D. Lukin, Phys. Rev. Lett. **98**, 123601 (2007); A. V. Gorshkov, A. André, M. D. Lukin, and A. S. Sorensen, Phys. Rev. A **76**, 033805 (2007).
[14] A. Dantan and M. Pinard, Phys. Rev. A **69**, 043810 (2004).
[15] J. Nunn, I. A. Walmsley, M.G. Raymer, K. Surmacz, F.C. Waldermann, Z. Wang, and D. Jaksch, Phys. Rev. A **75**, 011401(R) (2007).
[16] M. T. L. Hsu, G. Hétet, O. Glöckl, J. J. Longdell, B. C. Buchler, H.-A. Bachor, and P. K. Lam, Phys. Rev. Lett. **97**, 183601 (2006).
[17] D. Akamatsu, K. Akiba, and M. Kozuma, Phys. Rev. Lett. **92**, 203602 (2004).
[18] D. Akamatsu, Y. Yokoi, T. Tanimura, A. Furusawa, and M. Kozuma, e-print arXiv:quant-ph/0611097 (2006).
[19] J. Appel, E. Figueroa, and D. Korystov, and A. I. Lvovsky, e-print arXiv:0709.2258v2.
[20] K. Honda, D. Akamatsu, M. Arikawa, Y. Yokoi, K. Akiba, S. Nagatsuka, T. Tanimura, A. Furusawa, and M. Kozuma, e-print arXiv:0709.1785.
[21] T. C. Ralph and P. K. Lam, Phys. Rev. Lett. **81**, 5668 (1998).
[22] T. C. Ralph, P. K. Lam, and R. E. S. Polkinghorne, J. Opt. B: Quantum Semiclassical Opt. **1**, 483 (1999).
[23] W. P. Bowen, N. Treps, B. C. Buchler, R. Schnabel, T. C. Ralph, Hans-A. Bachor, T. Symul, and P. K. Lam, Phys. Rev. A **67**, 032302 (2003).
[24] A. Peng, M. Johnsson, W. P. Bowen, P. K. Lam, H.-A. Bachor and J. J. Hope, Phys. Rev. A **71**, 033809 (2005); G. Hétet, A. Peng, M. T. Johnsson, M. T. L. Hsu, O. Glöckl, P. K. Lam, H.-A. Bachor, and J. J. Hope, *ibid.* **74**, 059902(E) (2006).
[25] A. B. Matsko, Y. V. Rostovtsev, O. Kocharovskaya, A. S. Zibrov, and M. O. Scully, Phys. Rev. A **64**, 043809 (2001).
[26] A. S. Zibrov, A. B. Matsko, O. Kocharovskaya, Y. V. Rostovtsev, G. R. Welch, and M. O. Scully, Phys. Rev. Lett. **88**, 103601 (2002).
[27] A. Dantan, A. Bramati, and M. Pinard, Phys. Rev. A **71**, 043801 (2005).
[28] M. Martinelli, P. Valente, H. Failache, D. Felinto, L. S. Cruz, P. Nussenzveig, and A. Lezama, Phys. Rev. A **69**, 043809 (2004).
[29] V. A. Sautenkov, Y. V. Rostovtsev, and M. O. Scully, Phys. Rev. A **72**, 065801 (2005).
[30] P. Barberis-Blostein and N. Zagury, Phys. Rev. A **70**, 053827 (2004).
[31] S. E. Harris, Phys. Rev. Lett. **70**, 552 (1993).
[32] M. Fleischhauer, Phys. Rev. Lett. **72**, 989 (1994).
[33] E. Figueroa, F. Vewinger, J. Appel, and A. I. Lvovsky, Opt. Lett. **31**, 2625 (2006).
[34] P. D. Drummond and C. W. Gardiner, J. Phys. A **13**, 2353 (1980).
[35] C. W. Gardiner, *Handbook of Stochastic Methods*, 2nd ed. (Springer, Berlin, 1985).
[36] G. Collecutt, P. D. Drummond, P. Cochrane, and J. J. Hope, eXtensible Multi-Dimensional Simulator, documentation and source code available from http://www.xmds.org
[37] C. Cohen-Tannoudji, J. Dupon-Roc, and G. Grynberg, *Atom-Photon Interactions* (Wiley, New York, 1992).
[38] A. L. Gaeta, R. W. Boyd, and G. S. Agarwal, Phys. Rev. A **46**, 4271 (1992).
[39] C. M. Caves, Phys. Rev. D **26**, 1817 (1982).
[40] J. R. Jeffers, N. Imoto, and R. Loudon, Phys. Rev. A **47**, 3346 (1993).
[41] K. Hammerer, M. M. Wolf, E. S. Polzik, and J. I. Cirac, Phys. Rev. Lett. **94**, 150503 (2005).
[42] S. L. Braunstein, C. A. Fuchs, and H. J. Kimble, J. Mod. Opt. **47**, 267 (2000).
[43] F. Grosshans and P. Grangier, Phys. Rev. A **64**, 010301(R) (2001).
[44] H. Jeong, T. C. Ralph, and W. P. Bowen, J. Opt. Soc. Am. B **24**, 355 (2007).
[45] P. Grangier, J. A. Levenson, and J. P. Poizat, Nature (London) **396**, 537 (1998).
[46] M. D. Reid and P. D. Drummond, Phys. Rev. Lett. **60**, 2731 (1988).
[47] A. B. Matsko, D. V. Strekalov, and L. Maleki, Opt. Express **13**, 2210 (2005).
[48] T. Coudreau, F. Grosshans, S. Guibal, and L. Guidoni, J. Phys. B **40**, 413 (2007).
[49] P. D. Drummond, Comput. Phys. Commun. **29**, 211 (1983).
[50] P. D. Drummond, Opt. Commun. **49**, 219 (1984).
[51] A. B. Matsko, I. Novikova, M. O. Scully, and G. R. Welch, Phys. Rev. Lett. **87**, 133601 (2001).